AWESOME

WATER-ECOSYSTEM-FOOD

ROBUST ANALYSIS OF WEF PLANNING PORTFOLIOS

August, 2023

This project is part of the PRIMA Programme supported by the European Union, having received funding from it under grant agreement No 1942

PRIMA PARTNERSHIP FOR RESEARCH AND INNOVATION IN THE MEDITERRANEAN AREA

Programme Call:	PRIMA Call 2019 Section 1 Farming RIA
Project Number:	1942
Project Title:	AWESOME
Partners:	POLIMI (Project Coordinator), AUEB, YVC, UH, AF, RWTH, FEEM
Work-Package:	WP4
Deliverable #:	D4.4
Deliverable Type:	Document
Contractual Date of Delivery:	31 August 2023
Actual Date of Delivery:	31 August 2023
Title of Document:	Robust analysis of WEF planning portfolios
Author(s):	Veronica Piuri, Matteo Giuliani, Elena Matta, Arianna Leoni, George Papagiannis, Athanasios Yanncopoulous, Phoebe Koundouri, Martina Sardo, Davide Danilo Chiarelli, Maria Cristina Rulli, Giorgio Guariso, Andrea Castelletti
Content of this report:	Report about the robust analysis of the WEF planning portfolios under a wide range of uncertain future scenarios, including the introduced adaptation options and the identification of the most critical future conditions.
Availability:	This report is public.

Document revisions		
Author	*Revision content*	*Date*
Veronica Piuri, Matteo Giuliani	Table of content	06-07-2023
Veronica Piuri, Arianna Leoni, Elena Matta, Matteo Giuliani, Giorgio Guariso, Andrea Castelletti	First draft (v1)	31-07-2023
Ruslana R Palatnik, Lydia Stergiopoulou	Internal revision	10-08-2023
Veronica Piuri, Matteo Giuliani	Revised draft (v2)	23-08-2023

Table of Content

Table of Content 3
LIST OF ACRONYMS 4
EXECUTIVE SUMMARY 5
1. INTRODUCTION 6
2. ROBUST DECISION-MAKING FRAMEWORK 7
3. FUTURE SCENARIOS 9
3.1 NOMINAL SCENARIO 9
3.2 UNCERTAIN SCENARIOS 9
4. RESULTS 15
4.1 Robust portfolios against future scenarios 15
4.2 Pandemic risk 24
5. CONCLUDING REMARKS 27
6. REFERENCES 28

LIST OF ACRONYMS

Abbreviations

ANN: Artificial Neural Network
D: Deliverable
DAF: Decision-Analytic Framework
ECDF: Empirical Cumulation Density Function
GERD: Grand Ethiopian Renaissance Dam
HAD: High Aswan Dam
HBV: Hydrologiska Byrans Vattenbalansavdelning
MER: Merowe dam
NRB: Nile River Basin
RCP: Representative Concentrated Pathway
SSP: Shared Socioeconomic Pathway
T: Task
WEF: Water Energy Food
WEFE: Water Energy Food Environment
WP: Work Package

EXECUTIVE SUMMARY

Deliverable 4.4 describes the robustness analysis of the Water-Energy-Food planning portfolios under a wide range of future uncertain scenarios. It summarises the framework to implement a robust decision-making and describes the approach to generate the large ensemble of future scenarios. The document includes the analysis of the results obtained from the simulation of two efficient portfolios, identified in D4.3, under different future scenarios of water uses and water availability. The robustness of the two portfolios is assessed by the performance of the indicators defined in D4.2 for different future realisations of population growth, irrigation demand and hydroclimatic conditions. Our results show a large variation in indicators reflecting the magnitude of the scenarios generated, with the Egyptian water deficit being the sector most affected by future conditions of population growth and water scarcity. The total inflow of the Nile River is the main factor influencing the future hydroelectric production of Ethiopia, Sudan and Egypt, as well as the deficit of the latter two. The introduction of measures to reduce Egyptian water demand, such as reuse, groundwater, desalination and aquaponics bring benefits in most generated future conditions even if they result undersized for the most extreme scenarios. In addition to benefiting the water supply of the country, our research shows that the introduction of aquaponics in urban centres can make food production more robust to extreme events such as pandemics and lockdowns.

1. INTRODUCTION

Deliverable 4.4 (Robust analysis of Water-Energy-Food (WEF) planning portfolios) is the report about the robust analysis of the WEF planning portfolios under a wide range of uncertain future scenarios. The work is an outcome of Task 4.4 that explores the robustness of the WEF planning portfolios against a wide range of uncertain and challenging future hydroclimatic and socio-technological scenarios, possibly including new adaptation options to obtain a set of adapted solutions that perform satisfactorily across the set of future uncertain scenarios. State-of-the-art scenario discovery will be used for identifying critical future conditions under which a candidate portfolio becomes vulnerable to failure.

The broader goal of WP4 is to develop a Decision-Analytic Framework (DAF) running at the river basin scale. The DAF allows to simulate existing water availability, water distributions system and new agricultural technologies, based on hydrological models and combined with the results of systems analysis methods with advanced a-posteriori multi-objective optimization algorithms. The workflow of WP4 and its interconnections with the other WPs are illustrated in Figure 1. It relies on a detailed characterization of different innovative technological solutions demonstrated in WP5 at the micro-level (e.g., aquaponics) and a realistic representation of macroscale processes and regional policies influencing river basin dynamics in terms of land use, water and energy supply, and ecosystem services (WP2, WP3). Besides, the case study assessments and participatory processes initiated by WP6 support our activities, integrating stakeholders' views and interests to shape our analyses.

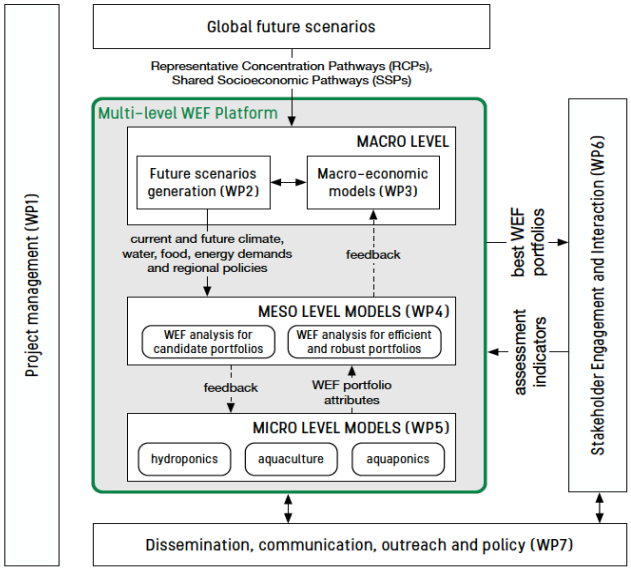

Figure 1 – AWESOME project structure

The DAF employs a strategic river model coupled with an optimization engine (for details, see Deliverable 4.3): the river model is a parsimonious model conceptualizing the main natural processes and human decisions at the whole river basin scale. The optimization engine implements a simulation-based optimization via multi-objective evolutionary algorithms[1], which iteratively

improves a set of candidate solutions in terms of their performance, estimated via simulation of the strategic model, with respect to a subset of selected evaluation indicators (i.e. design indicators). The strategic model developed for the Nile River Basin (NRB) integrates two main components: the water supply model and the water demand model. The former supports the analysis of the operating policies of the main dams along the Nile River, along with the water abstraction for the irrigation areas in Sudan and the water supply downstream of the High Aswan Dam (HAD). The water demand model investigates alternative combinations of water demand interventions, namely reuse, groundwater, aquaponics/hydroponics and desalination, to reduce the water demand downstream of the HAD.

In this Deliverable, we evaluate the robustness of two efficient planning portfolios adapted to a future scenario representing a nominal projection of the conditions around the middle of the century (see Deliverable 4.3) over a large ensemble of future scenarios of water demand and water availability. We also address the robustness of the identified portfolios concerning the pandemic risk.

The Deliverable is structured as follows: the next section describes the robust decision making framework by[2] and how this is implemented for the identification of robust adaptation pathways; Chapter 3 summarizes scenarios, and efficient pathways for the NRB; and Chapter 4 discusses the corresponding results; the final remarks are presented in the last chapter.

2. ROBUST DECISION-MAKING FRAMEWORK

Understanding the capacity of various solutions to handle uncertain changes, both in terms of climate and human factors(e.g., extreme precipitation events, severe drought, rapid urbanization, and the expansion of intensive agriculture) is crucial in designing resilient adaptation pathways. In this context, robustness can be defined as *"the insensitivity of system design to errors, random or otherwise, in the estimates of those parameters affecting design choice"*[3]. A robust decision, therefore, strives to minimize sensitivity to uncertainty and ensure consistent performance across multiple plausible futures. Extensive research has demonstrated that decision makers are willing to prioritize the robustness of selected solutions over expected performance[4–6]. In this section, we illustrate the taxonomy of robustness frameworks proposed by[2] that we used for assessing the robustness of the selected portfolios in the NRB.

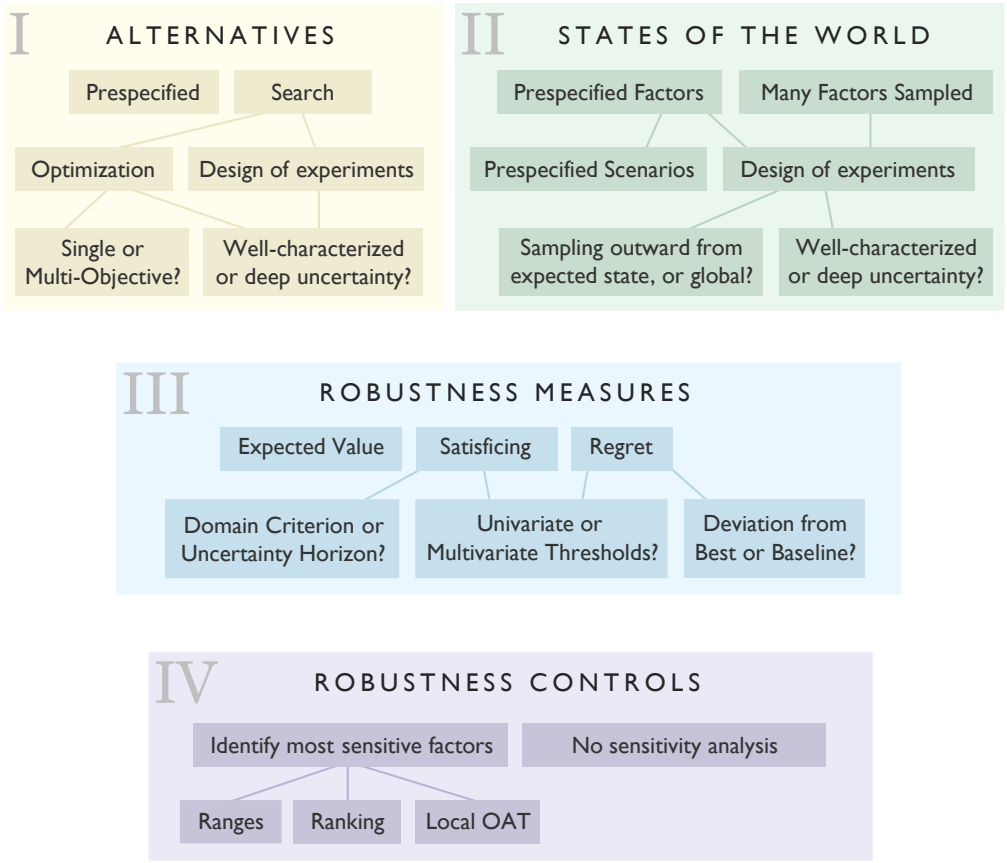

Figure 2 – Taxonomy of robustness frameworks[2].

The taxonomy of robustness frameworks reported in Figure 2 provides a comprehensive summary of existing approaches, that can be classified based on the methods adopted for (1) the generation of decision alternatives; (2) the generation of scenarios (i.e., states of the world); (3) the quantification of robustness; (4) the scenario discovery to identify the most important factors (i.e., robustness control).

In this context, the first step focuses on the identification of decision alternatives. These alternatives can either be pre-specified by the decision-makers, especially in simple cases with a discrete set of options[7,8]. Alternatively, computational search[9] and optimization methods[10] can be employed to generate alternatives by exploring the decision space. Optimization enables decision-makers to incorporate computational simulations to better understand the future performance of the designed solutions. In our case study of the NRB we generate our alternatives via optimization as reported in Deliverable 4.3. The second step of the framework involves evaluating the performance of the identified alternatives across a diverse set of uncertain states of the world, also known as scenarios. These scenarios are constructed by considering different combinations of uncertain factors that might influence the outcomes. To create an ensemble of scenarios, various techniques can be used, such as pre-specifying scenarios[11], sampling from noninformative priors, or using well-characterized probability distributions where available[12]. In this deliverable, we generate the future scenarios starting from RCPs and SSPs projections, see Chapter 3 for more information.

The framework's third step is concerned with quantifying the robustness of the decision alternatives. Different robustness metrics can be employed to capture the degree of pessimism or optimism of the decision-makers[13]. These metrics include expected value metrics[14], higher-order moments (e.g., variance and skew)[15], regret-based metrics[16], and satisficing metrics[17]. Each of these metrics offers unique insights into the performance of the alternatives under different conditions. In this work, rather than using a single prespecified performance threshold, we explored the broader implications of alternative performance requirements by visualizing the robustness metric for any performance threshold. After quantifying the robustness of candidate alternatives, the last step is the scenario discovery analysis to isolate the uncertain factors most responsible for the system failure. This step can be considered as a consequence-oriented sensitivity analysis[2], which is also known as factor mapping[18].

3. FUTURE SCENARIOS

3.1 NOMINAL SCENARIO

In Deliverable 4.3, we optimized the water supply model using future projections of inflows and irrigation and municipal demand according to the RCP4.5 and SSP2 scenarios for the middle of the century. Specifically, we obtained the future inflows of the four main tributaries of the Nile (Blue Nile, White Nile, Tekeze-Atbara, Dinder-Rahad) using the Hydrologiska Byråns Vattenbalansavdelning (HBV) model[19], a lumped rainfall-runoff model, combined with a neural network to improve its performance. Furthermore, within the work carried out by WP2, future population growth projections were obtained under the Bayesian population model developed by[20,21], and the crop water requirements were estimated using the spatially distributed agro-hydrological model WATNEEDS [22].

From the results obtained in Deliverable 4.3, we selected two portfolios that represent a compromise between the different sectors considered, in particular between hydroelectric production at the basin scale and water deficits in Egypt and Sudan. The two nominal solutions are referred to as *low reduction* and *medium reduction* solutions, as they respectively foresee the implementation of low and medium efforts for the reduction of Egypt's water use.

3.2 UNCERTAIN SCENARIOS

For the generation of the uncertain scenarios, in addition to considering the scenario pair RCP4.5-SSP2, representing an intermediate scenario of population growth and climate change, we considered the pairs RCP2.6-SSP1 and RCP8.5-SSP5. These scenarios represent a range of socio-economic and climate pathways, allowing us to capture a diverse spectrum of potential impacts and inform robust decision-making.

The increase in municipal and industrial water use in Egypt is considered proportional to the increase in population. This is calculated in Deliverable 2.1 for the scenarios SSP1, SSP2 and SSP5 with the Bayesian population model which produces probabilistic projections for the population pyramids of both genders. This model is a stochastic extension in a Bayesian fashion of the typical logistic-type model used by the United Nations for predicting population and it relies on three main modelling components: (a) fertility rate, (b) life expectancy and (c) migration. Figure 3 shows the percentage of population growth under the three SSPs scenarios between the 10th and 90th

percentile. Under the SSP1 and SSP5 scenarios, a very similar population increase occurs, such that they cannot be distinguished in Figure 3, while the SSP2 scenario is characterized by a higher population increase.

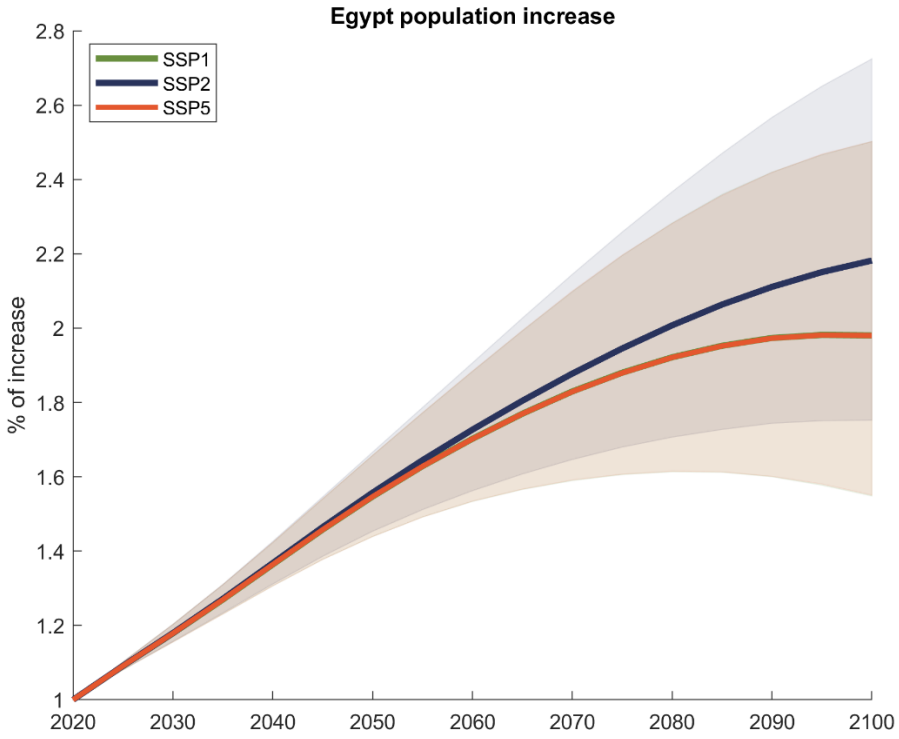

Figure 3 – Percentage of increase in Egypt's population from 2020 to 2100. The coloured areas show the percentage of population increase for the three scenarios SSP1, SSP2 and SSP3 between the 10th and 90th percentile, the darker lines indicate the median. The projections for SSP1 and SSP5 overlap and it is therefore not possible to see the green area.

Crop water use of Egypt and Sudan are estimated in Deliverable 2.3 under the three couples of climate projections and population growth (RCP2.6-SSP1, RCP4.5-SSP2 and RCP8.5-SSP5), considering different options of crop distribution. Specifically, we used the spatially distributed agro-hydrological model WATNEEDS[22] to assess the daily water balance and the volumes of water needed to cover crop's evapotranspiration during the growing period without experiencing water stress. Green water requirement is met by precipitation, while blue water requirement is met by irrigation when precipitation alone cannot completely satisfy the crop requirement. In Egypt, four different water demand scenarios for each RCP-SSP pair are considered: one that considers the current diet and current yield (D0I0), one with current diet and yield intensification (D0I1), one with a balanced diet and current yield (D1I0) and the last with a balanced diet and yield intensification (D1I1). For Sudan, on the other hand, we consider only the results obtained at the basin scale according to two crop intensification scenarios: one with current yield (I0) and one with yield intensification (I1), since the results obtained at the national level report consumption of irrigation water higher than the current consumption (up to 50%), resulting in a non-sustainable scenario in terms of water consumption. To have a wide enough range (Figure 4) from which to extract values for the robustness analysis, we assumed that future demand for the irrigation sectors of Egypt and

Sudan will lie within the different water demands defined by the different diet and crop intensification scenarios. The projections in 2100 show that in Egypt the highest water use is expected for the RCP8.5-SSP5 scenario, and the lowest for RCP2.6-SSP1. In Sudan, the scenario with the highest demand is RCP4.5-SSP2, while RCP8.5-SSP5 is the lowest, with the RCP2.6-SSP1 scenario covering a very wide range of values that includes the demands of the other two scenarios. In Sudan, the scenario RCP8.5-SSP5 shows the lowest water requirements, associated with higher precipitation and a lower difference between the average maximum and minimum temperatures at the basin scale, with respect to the other scenarios. There is a substantial difference between the future water use scenarios for the two countries. As can be seen in Figure 4, Sudanese demand requires smaller volumes of water than the Egyptian one. Furthermore, the two uses have a very different time distribution, with Egyptian demand having a summer peak, while Sudanese demand has both a summer and an autumn peak. Finally, the realisations of the future scenarios differ between the two states, with the RCP8.5-SSP5 scenario being the worst for Egypt and RCP4.5-SSP2 and RCP2.6-SSP1 being the worsts for Sudan. This last difference may generate conflicting results in the simulation of the future deficits of the two countries, which we would expect to be high in Egypt for the RCP8.5-SSP5 scenario and high in Sudan for the RCP2.6-SSP1 and RCP4.5-SSP2 scenarios.

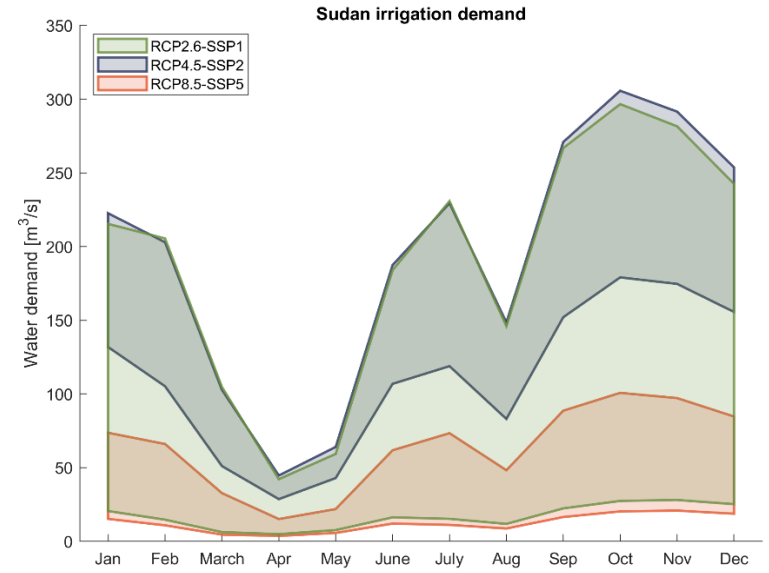

(a)

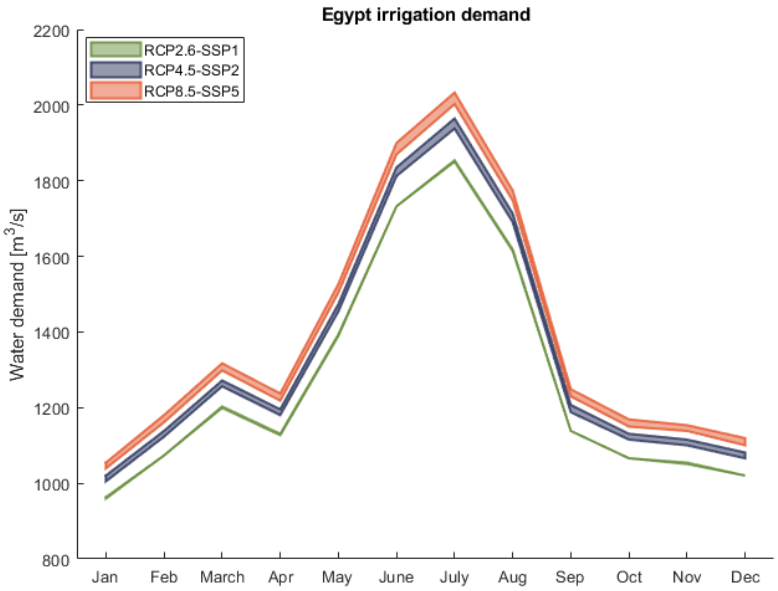

(b)

Figure 4 – Sudan (a) and Egypt (b) monthly irrigation water demand projection in 2100. The coloured areas indicate the ranges between the scenarios of different diets and crop intensification.

The streamflow projections of the four main tributaries of the Nile are obtained by the process described in Deliverable 4.3. We used the HBV model[19], which takes as inputs temperature and precipitation values to generate streamflows. By feeding to the model bias adjusted and downscaled values of temperature and precipitation for three different RCPs (RCP2.6, RCP4.5 and RCP8.5) we obtained inflows projections according to the three scenarios. The projections were then improved by an Artificial Neural Network (ANN) since the HBV could not correctly emulate the inflows peaks. With this procedure, we obtained three projected time series of future streamflows from 2007 to

2100 for the four Nile tributaries (Figure 5). According to projections obtained at the end of the century, the RCP8.5 scenario shows a greater reduction in runoff compared to the other two projections. This behaviour replicates the trend of projected precipitations that in the area are expected to decrease especially for the RCP8.5 scenario.

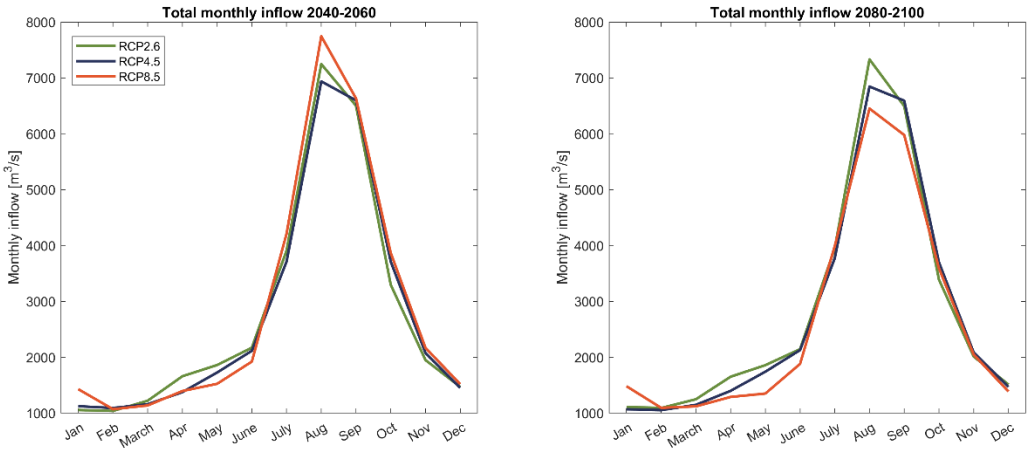

(a) (b)

Figure 5 - Cyclostationary mean of the total inflows of the combined four Nile tributaries between (a) 2040 -2060 and (b) 2080 - 2100.

To obtain a large ensemble of future streamflow scenarios, we generate from the three RCPs projection 100 synthetic realisations of the streamflow time series for each RCP. To achieve this, we rescaled the RCPs projection using the method described in[23]. The main objective of the scaling process is to find a vector of monthly multipliers to apply to the RCPs time series projections of inflows. First, we perform a logarithmic transformation of the RCPs inflow time series to formulate time series of normally distributed monthly flows, Y = ln(Q), where Q is the RCPs inflow time series. We then standardise Y to generate sets of standardised normal monthly flows, Z, as shown in the following equation:

$$Z_{i,j} = \frac{Y_{i,j} - \hat{\mu}_j}{\hat{\sigma}_j}$$

where $\hat{\mu}_j$ and $\hat{\sigma}_j$ are the sample mean and sample standard deviation of the log-transformed RCPs monthly flows projection of the j-th month.

To rescale the monthly Q flows in alternative Q' flow scenarios, variable monthly mean multiplier vectors M_μ = [$M_{\mu,1}$,..., $M_{\mu,12}$] and standard deviation multipliers M_σ = [$M_{\sigma,1}$,..., $M_{\sigma,12}$] are applied to $\hat{\mu}_j$ and $\hat{\sigma}_j$ respectively, when back-transforming Z, as shown in equation:

$$Q'_{i,j} = \exp\left(M_{\mu j}\,\hat{\mu}_j + M_{\sigma j}\,\hat{\sigma}_j Z_{i,j}\right)$$

The monthly multipliers are generated to model smooth and continuous changes in seasonality with a limited number of parameters. We fit the Fourier series to logarithmic monthly mean inflows and compute time-varying multipliers by dividing the monthly averages predicted by an adjusted harmonic, y_2, with respect to those predicted by the RCPs fit, $\widehat{y_1}$. The monthly averages of logarithmic-scale flow in each of the four Nile tributaries can be modelled from the first two harmonics. Namely, the monthly averages of logarithmic-scale flows, $\widehat{y_1(\iota)}$, at each site can be described by equation:

$$\widehat{y_1(i)} = \bar{y} + C_1 \cos\left(\frac{2\pi i}{12} - \Phi_1\right) + C_2 \cos\left(\frac{2 * 2\pi i}{12} - \Phi_2\right)$$

where $\bar{y}$ is the mean of the RCPs time series of log-space monthly means, C_1 and Φ_1 are the amplitude and phase, respectively, of the first harmonic (i.e., annual cycle), C_2 and Φ_2 are the same for the second (i.e., semiannual cycle), and *i* is the month of the year. We create adjusted time series, y_2, for each site by applying multipliers to C_1 and/or C_2 and phase shifts to $\Phi_1$and/or Φ_2, thereby capturing changes in seasonality with only four parameters. The amplitude multipliers, m_{C_1} and m_{C_2}, and phase shift deltas, d_{Φ_1} and d_{Φ_2}, are used to calculate a new cycle of mean monthly flows, y_2, according to equation:

$$y_2(i) = \bar{y} + m_{C_1} C_1 \cos\left(\frac{2\pi i}{12} - (\Phi_1 - d_{\Phi_1})\right) + m_{C_2} C_2 \cos\left(\frac{2 * 2\pi i}{12} - (\Phi_2 - d_{\Phi_2})\right)$$

The *i*th element of M_μ and M_σ can then be calculated as $y_2(i)/\widehat{y_1(i)}$. In order to change the log-space mean annual flow simultaneous to the interannual distribution, the *i*th element of M_μ can be calculated according to equation:

$$M_{\mu,i} = [m_\mu y_2(i)/\widehat{y_1(i)}]$$

Using the method described above, we generated 100 synthetic inflows for each RCPs, for a total of 300 inflow scenarios from 2007 to 2100. Given their substantial size, the synthetic time series mostly overlap (see Figure 6), with the highest annual runoff averages recorded for some of the scenarios derived from the RCP8.5 projection. Across all projections, a general decline towards the end of the century is evident. This downward trend can be attributed to climate change patterns, characterized by rising temperatures and reduced precipitation.

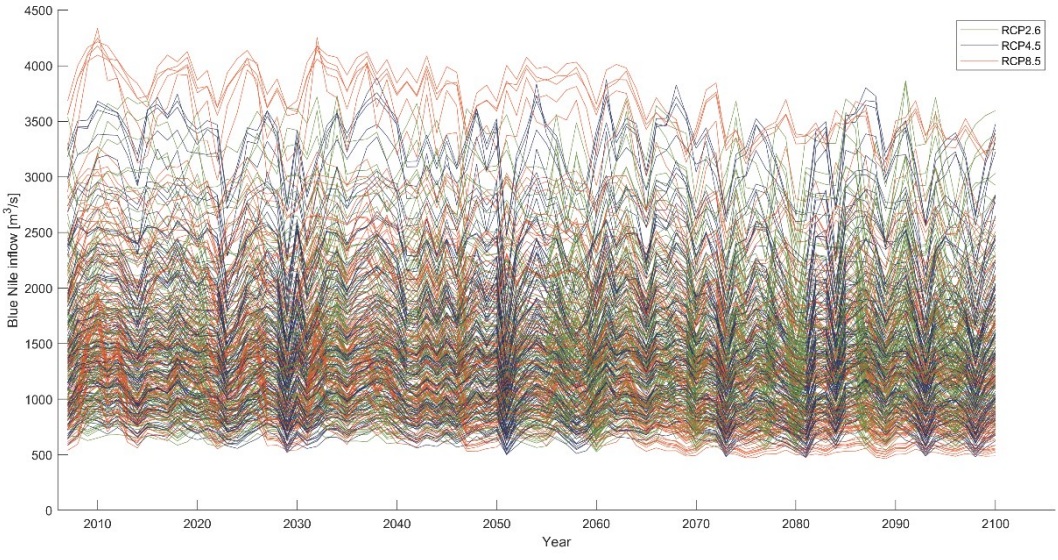

Figure 6 – Annual mean inflows of 300 synthetic streamflows of the Blue Nile generated from three RCPs projections from 2007 to 2100.

4. RESULTS

This section presents the robustness analysis for two efficient portfolios of the NRB operation, found in Deliverable 4.3, under the large ensemble of future scenarios of water availability and water use described in the previous Chapter, as well as the robustness to the pandemic risk for the solutions of the water demand system. The two portfolios represent two solutions of the Water Supply System that balance hydropower production at the basin scale (J^{E}), hydropower production in the Grand Ethiopian Renessaint Dam (GERD) ($J^{E,GERD}$), Merowe dam (MER) ($J^{E,MER}$) and HAD ($J^{E,HAD}$), water deficit in Egypt ($J^{Defict,Egypt}$) and irrigation deficit in Sudan ($J^{Irr,Sudan}$). The two portfolios are distinguished by the different extent of water demand reductions they implement in Egypt, hence the names *low water reduction* portfolio and *medium water reduction* portfolio. The second solution, thanks to greater reductions in Egyptian water demand, is able to achieve greater hydroelectric power production without significantly decreasing the two countries' deficits.

4.1 Robust portfolios against future scenarios

To assess the robustness of the two efficient portfolios, we implement a stratified sampling of the scenarios described in the previous section to guarantee consistency between hydroclimatic and socio-economic projections. Specifically, we first randomly sample a given RCP-SSP combination among the RCP2.6-SSP1, RCP4.5-SSP2 and RCP8.5-SSP5. Then, we coherently extract the streamflow scenarios from the union of the projections over the 2040-2060 and 2080-2100 horizons for the considered RCP, the future Egyptian population (and associated demand) increase from the 10^{th} and 90^{th} percentiles of the distributions in 2050 and 2100 for the considered SSP, and the irrigation demands of Egypt and Sudan within the range of the projections at 2100 for the considered combination of RCP-SSP. For the latter, we considered only the end of century projections as this range includes the one projected in 2050. In total, we simulated the two portfolios selected in Deliverable 4.3 over an ensemble of 500 different scenarios. These 500 scenarios, being randomly drawn from the set described in Chapter 3, retain the same properties as the latter.

Figure 7 reports the results obtained over the simulation of the two solutions for the 500 randomly selected scenarios, using a parallel-axes plot. In this representation, every line is a different simulation of the same portfolio under a different scenario, where each axe represents an indicator with the direction of preferences that is always upward. The solutions with performance less than the 10^{th} percentile of the objectives are cut to allow a better visualization of the obtained simulations, and the original performance of the two solutions is marked by a thick black line.

In the 500 simulations obtained, the performance of the various indicators vary greatly from the original values, especially for hydropower production and the deficit in Egypt. For both simulated solutions, the ranges of the six indicators are similar. In the solution with *medium reductions* (Figure 7b), we obtained higher maximum values of hydropower production both at the basin scale and for individual dams. This is because the nominal starting solution with medium reductions in Egyptian water use favoured higher hydropower production at the expense of a higher water deficit in both Egypt and Sudan compared to the solution with low reductions (Figure 7a). Both solutions have similar minimum Egypt's deficit values equal to zero or very close to zero, while lower maximum

values are registered in the solution with *medium reduction*, probably due to the greater reductions in the country's water demand that can keep the deficit at lower levels.

Finally, the Sudanese deficit has minimum values of zero for both solutions and higher maximums for the *medium reduction* solution, as the nominal solution had a higher deficit value. For hydropower, there are both large improvements and substantial deteriorations, with basin-scale hydropower production ranging from half to almost double the original performance. The individual production of GERD and HAD have a similar behavior to the total hydroelectric production with values ranging from half to twice the nominal solutions. The only exception is the MER production, which reaches a maximum value that exceeds the performance in nominal conditions by only 90 and 100 GWh/month, whereas the worst-case performance is about 50% of the nominal one. This is probably due to a technological limitation of this dam's plant, which is smaller compared to the ones of GERD and HAD. The Egyptian deficit shows large increases from an initial value of around 2 and 6 m^3/s in the nominal solutions to around 600 m^3/s in the simulations with the lowest performance. However, many solutions concentrate on lower deficit values. The deficit in Sudan undergoes much smaller changes than the other indicators.

These results are easily explained by the wide range of scenarios used in the simulation, especially the wide ranges of synthetic inflows, which directly influence hydropower production, and the high population growth in Egypt that affects the deficit of the country. On the contrary, the scenarios of irrigation demand in Sudan are almost always lower than under the nominal projections, favoring a reduction of the deficit when simulated over the considered ensemble of scenarios.

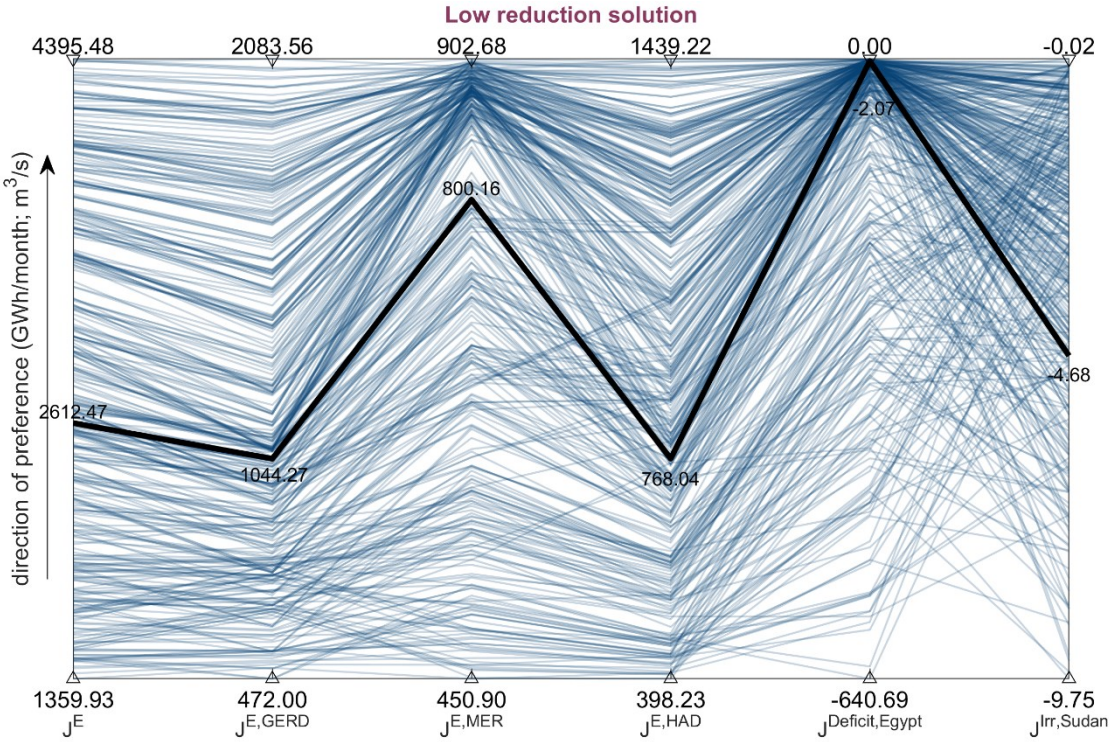

(a)

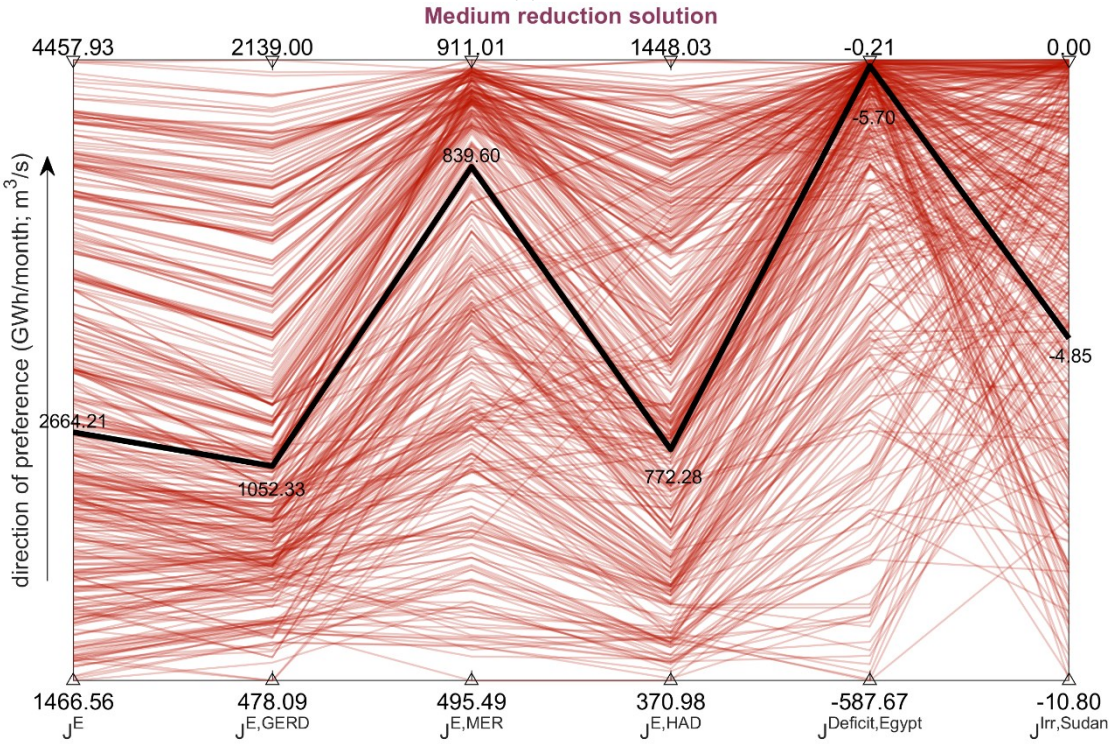

(b)

Figure 7 – Simulation performance of the water supply indicators for the two nominal solutions *low* (a) and *medium reduction* (b). The original performances of the two solutions are highlighted in black.

Figure 8 shows the distribution of the performance attained by the two portfolios over the large ensemble of future scenarios by using violin plots. A violin plot is a graphical representation used to visualize the distribution of a continuous variable across different categories or groups. It combines aspects of a box plot and a kernel density plot to provide a more detailed view of the data distributions. Each "violin" in the plot represents a category, and its width is proportional to the density of data points at different values.

In Figure 8, we grouped the solutions according to the different RCP-SSP scenarios, while the distinction between the two different solutions is given by the colour, blue for the *low reduction* and red for the *medium reduction* solutions. The distribution of hydropower production (Figure 8a) is uniform across the entire range of the indicator and across the different scenarios. This is shown by the shape of the "violin", which has the same width over the whole area. This confirms the perception from the parallel plot (Figure 7), where the lines are evenly distributed around the range of the hydropower objectives. Almost no difference is observed in the three RCPs-SSPs scenarios, which is easily explained by looking at the inflow scenarios: the synthetic ensembles generated from the three RCPs overlap for the most part (see Figure 6). As hydropower production is strongly related to the Nile inflow, it also exhibits a similar distribution across all three scenarios. The main difference between the three scenarios is a slight decrease in the median from RCP2.6-SSP1 to RCP8.5-SSP5, indicated by the horizontal line of boxplots within the violins. Again, the explanation for this behaviour can be found in the distribution of the inflows scenarios: although these are distributed similarly for the three scenarios, the three original RCP series show higher inflow values for the RCP2.6 scenario and lower values for RCP8.5 (see Figure 5b).

The distribution of the two deficit indicators shows greater differences when moving between the three RCPs-SSPs scenarios. Looking at the distribution of the deficit in Egypt (Figure 8b), the most robust scenario is RCP2.6-SSP1, which shows the highest density of deficit values close to zero. For the other two scenarios, it is still observed that most solutions are concentrated around low deficits, but with higher densities for higher values, as well as higher median values and higher maximum values compared to the RCP2.6-SSP1 scenario. This can be explained by the distribution of Egypt's water demand scenarios. The lowest increase in water demand is expected for both irrigation and municipal water demand is projected under RCP2.6-SSP1, whereas RCP8.5-SSP5 is associated with the highest increase in irrigation water demand and in RCP4.5-SSP2 with the highest increase in municipal water demand, respectively. Finally, Sudan's deficit (Figure 8c) is also mostly distributed around zero, with the difference that the RCP8.5-SSP5 scenario is the most robust, as the simulated deficit for this scenario is lower than for the other two probably because of the low demands projected under this scenario.

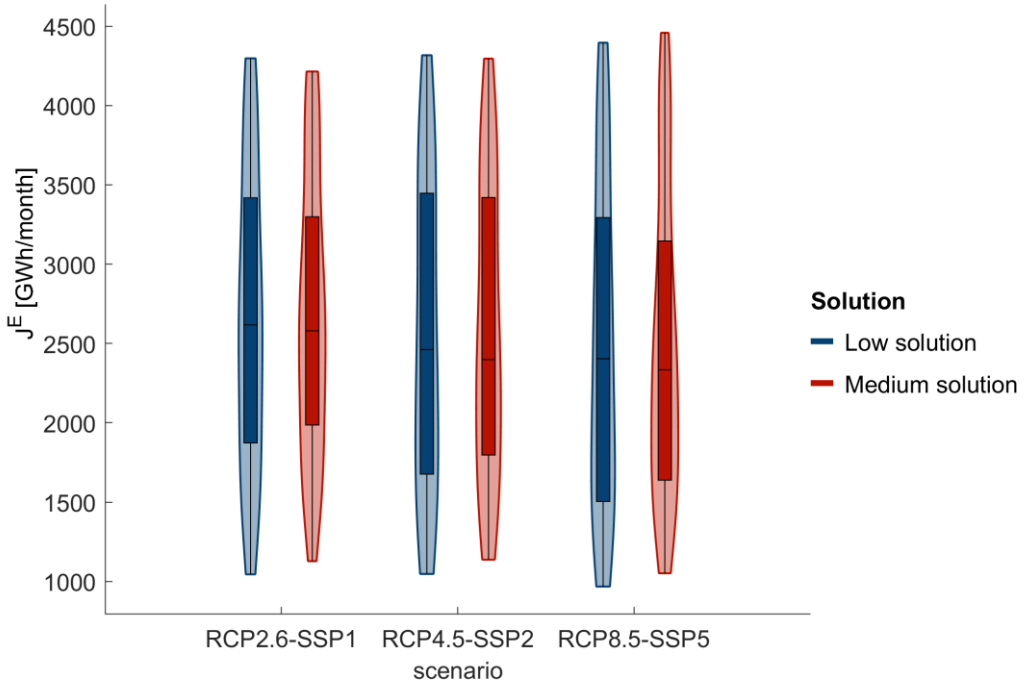
4500
4000
3500
3000
2500
2000
1500
1000
J^E [GWh/month]
RCP2.6-SSP1
RCP4.5-SSP2
RCP8.5-SSP5
scenario
Solution
Low solution
Medium solution

(a)

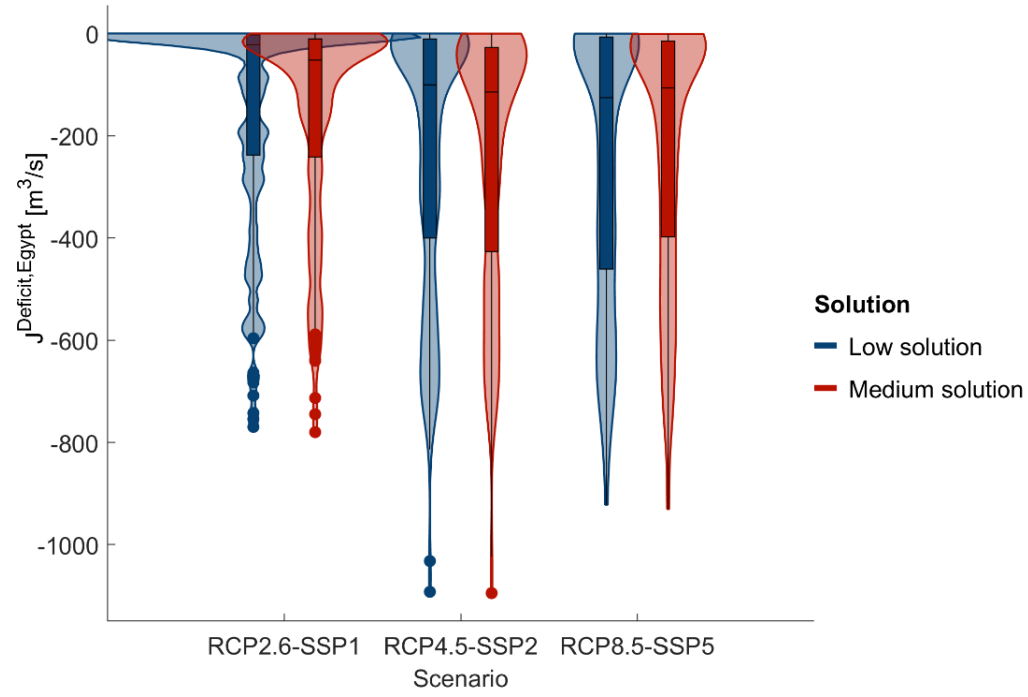
0
-200
-400
-600
-800
-1000
$J^{Deficit,Egypt}$ [m^3/s]
RCP2.6-SSP1
RCP4.5-SSP2
RCP8.5-SSP5
Scenario
Solution
Low solution
Medium solution

(b)

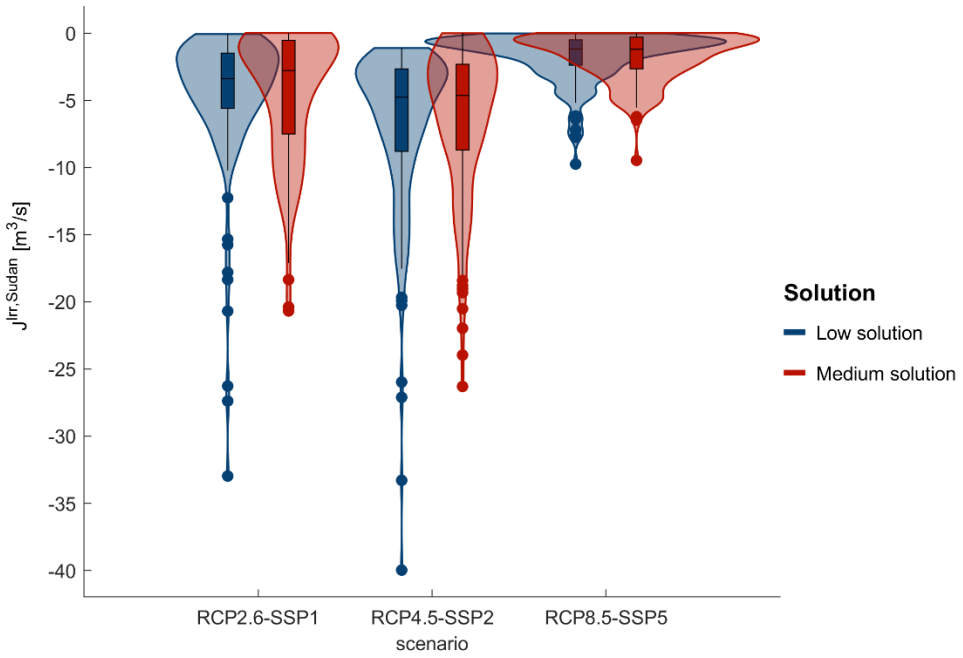

(c)

Figure 8 – Violin plot of (a) hydropower production at the basin scale (J^E), (b) Egypt's water deficit ($J^{Deficit,Egypt}$) and (c) Sudan's irrigation deficit ($J^{Irr,Sudan}$). In blue are plotted the simulations obtained from the *low reduction* solution and in red the ones obtained from the *medium reduction* solution.

Figure 9 shows the Empirical Cumulation Density Functions (ECDFs) for the three indicators measuring hydropower production, Egypt's deficit and Sudan's deficit. The vertical axis shows the percent of solutions that achieve or exceed the performance indicated in the horizontal axis, where the most desirable indicator values are shown at the leftmost corner. The values of the indicators of the nominal solutions are marked as vertical dashed lines. The two portfolios (blue and red lines) have similar ECDF values across the three indicators, suggesting that the selected solutions are equally robust/vulnerable. Looking at the performance of hydropower production (Figure 9a) between 55% and 60% of the simulations perform worse than the nominal solutions. In general, the ECDF of this indicator varies linearly, indicating the vulnerability of this sector with respect to future uncertain conditions. Both portfolios are more robust in terms of the Sudan deficit (Figure 9b): the two fairly vertical ECDFs show that approximately 30% of the simulations attain a worse performance than under nominal conditions, and in only 5% of the considered scenarios we obtain a deficit greater than 20 m^3/s. In contrast, the Egyptian deficit (Figure 9c) results in the maximum vulnerability, as illustrated by the relatively straight ECDFs for about the best 35% of the simulations, which then deteriorate rapidly. Only 10% of the simulations improve or have a deficit equal to the nominal performance of the efficient portfolios.

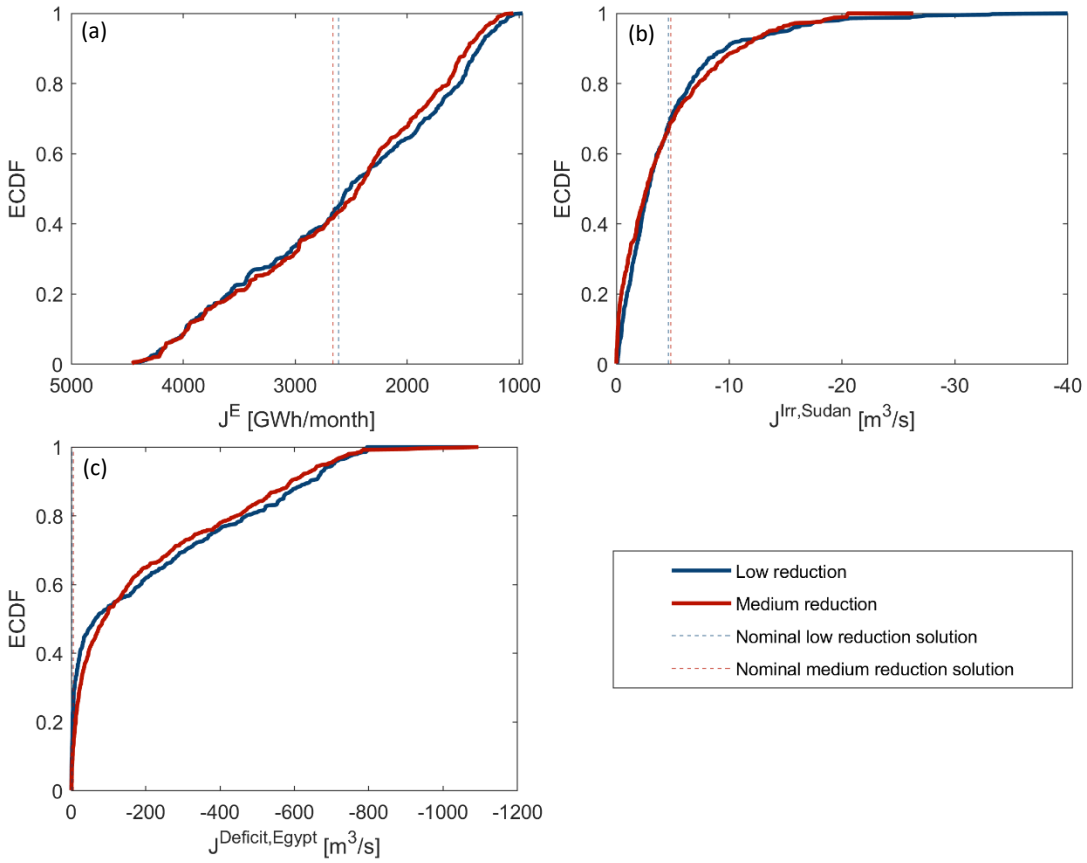

Figure 9 – Empirical Cumulation Density Functions (ECDFs) of hydropower production at the basin scale (J^E), (b) Egypt's water deficit ($J^{Deficit,Egypt}$) and (c) Sudan's irrigation deficit ($J^{Irr,Sudan}$). The blue line indicates the simulations of the low reduction solution, while the red line the simulation of the medium reduction solution. The dashed lines indicate the original performance of the two solutions.

Lastly, we perform the scenario discovery analysis by visually investigating the distribution of the indicators values with respect to the projected inputs characterizing the considered ensemble's members (Figure 10). For both solutions, there are similar relationships between indicators and variables. The hydropower production of GERD (Figure 10a) is proportional to the inflow of Blue Nile. This dam is in fact located on this tributary and has no other upstream elements in our model; its hydropower production will therefore depend directly on the water volumes of this river. The production of the MER (Figure 10b) and HAD (Figure 10c) is proportional to the total inflow of the Nile, as these two dams are located on the Main Nile and their production depends on the combination of the four tributaries of the Nile. Again, as inflows increase, hydroelectric production increases.

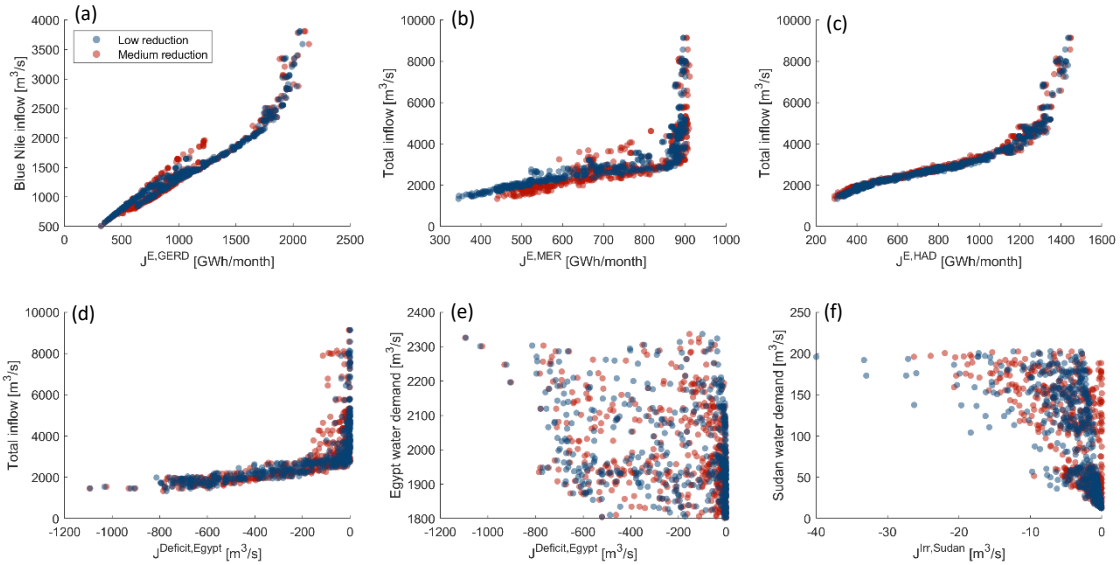

Figure 10 – Scatter plot of inputs variables against indicators for the low reduction solution simulations (blue) and medium reduction solution simulations (red). (a) Blue Nile inflow against hydropower production of GERD ($J^{E,GERD}$); (b) Total inflow against hydropower production of MER ($J^{E,MER}$); (c) Total inflow against hydropower production of HAD ($J^{E,HAD}$); (d) Total inflow against Egypt's deficit ($J^{Deficit,Egypt}$); (e) Egypt water demand against Egypt's deficit ($J^{Deficit,Egypt}$); (f) Sudan water demand against ($J^{Irr,Sudan}$).

The deficit in Egypt (Figure 10d) also shows a correlation with the total inflow. Looking at the scatterplot, we can identify a sort of inflow threshold above which the deficit remains low, while the indicator starts to decrease linearly when the projected inflow falls below this threshold. With a simple regression line (Figure 11), we identified this critical threshold as a total streamflow equal to 2776 m^3/s. This value represents a safety threshold above which we can expect a low value of the deficit. If future climate change conditions will lead to a lowering of the inflow below this level, then the NRB's operational system will have to be further adapted as the considered portfolios will become very inefficient.

As for the deficit in Sudan, it still shows slight relation with the total inflow but with less remark compared to the Egyptian one and their scatter plot is not reported here. Furthermore, the deficits of Egypt (Figure 10e) and Sudan (Figure 10f) do not show any particular trend with respect to the change in water demand, except that high deficits cannot occur for low water demands.

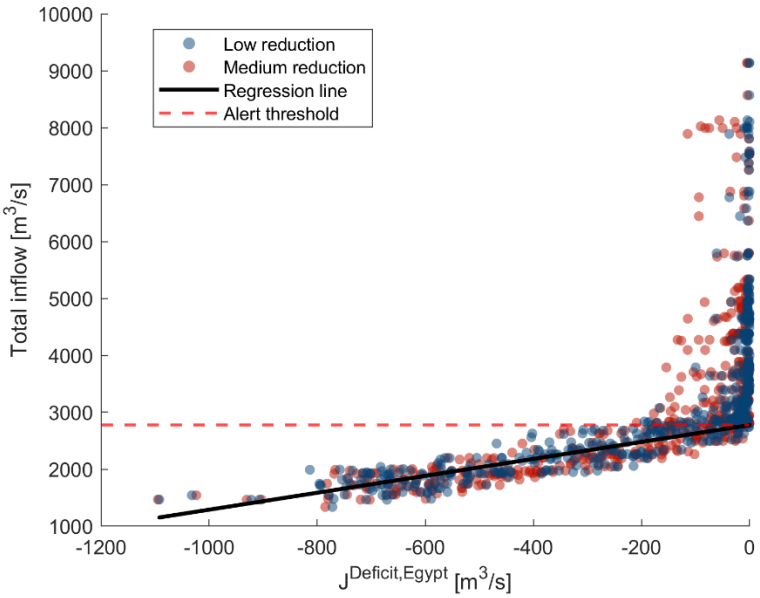

Figure 11 – Scatter plot of total Nile inflow against Egypt's deficit. The black line shows the regression line between the two variables while the red dashed line is the alert threshold.

Finally, let us analyse the variation of the expected water demand reduction in Egypt. This measure is strictly related to the planning of water intervention (groundwater, reuse, aquaponics and desalination) in Egypt. Figure 12 shows the ECDF of this indicator for the 500 simulations made for the *low reduction* and *medium reduction* solutions. The value of demand reduction of the two nominal solutions are marked by vertical lines. In both solutions, only about 15% of the solutions report a lower value of demand reduction than under the nominal conditions. In these scenarios, the planned water demand measures are oversized compared to the future demands and will generate larger water volumes that can contribute in further lowering the water supply deficit in Egypt with respect to the values reported in Figure 7. Yet, in 85% of our scenarios, the water demand reduction increases, making the planned water demand measures insufficient, likely requiring an additional increase of water reuse and groundwater extraction. In the worst-case, the *low reduction* portfolio will require an additional 25% of water demand reduction, which increases to 27% for the *medium reduction* one. In both cases, these increases in water demand reduction do not exceed 30% of the original solution, indicating that the two considered efficient portfolios will be able to meet a large share of the projected water demand.

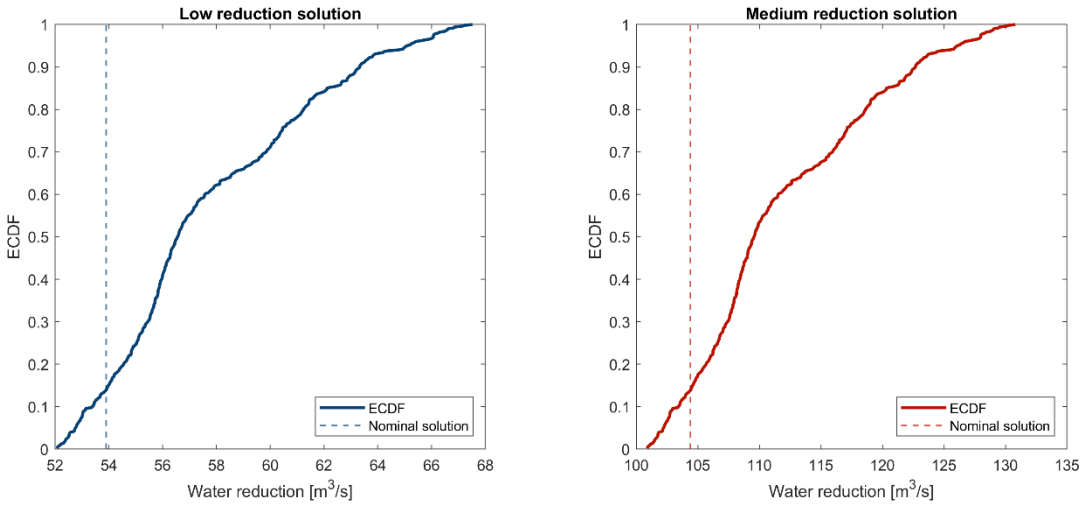

(a) (b)

Figure 12 – ECDF of the water reduction in the 500 simulations obtained for the nominal low reduction solution (a) and the medium reduction solution (b).

4.2 Pandemic risk

The recent COVID-19 outbreak has brought pandemic threats to the forefront of our society's awareness. With globalization and connectivity on the rise, these events are likely to increase in frequency as disease agents can rapidly spread across the globe within hours[24]. The impact of pandemics extends beyond the high death toll, it leads to widespread restrictions, lockdowns, and workforce disruptions, with shortages of critical resources like food becoming prevalent. By incorporating pandemic risk assessment and mitigation strategies into the strategic planning of water and food resources in the NRB, our work can achieve greater robustness and adaptability to face these unforeseen challenges.

With this in mind, we have included an indicator in our work that can assess the risk of a pandemic. This indicator (J^{Aq7} formulated in D4.2) computes the average distance of lettuce production from large urban centres. This value therefore indicates the distance of the most densely populated areas from the production of food and workplaces. In the context of future lockdowns caused by pandemics, we want this distance to be as short as possible to keep food and job resources close to densely populated areas. Up to now, in our work, we only evaluated the solutions with this indicator, without including it in the optimization. In the previous Deliverable 4.3 we found that the introduction of soilless agriculture can bring benefits with respect to pandemic risk, by locating part of Egypt's lettuce production close to Cairo, the most populated area in Egypt. To further improve the allocation of lettuce production and increase the robustness of the solutions to the pandemic risk, we re-optimised the system for the two targets of water reduction (*low* and *medium*) using the J^{Aq7} indicator as one of the objectives to be minimised in the water demand problem. By comparing the value of the J^{Aq7} indicator in the original and new optimisations (Figure 13), we see that the indicator is on average lower in the new optimisations, which therefore show more robustness with respect to pandemic risk.

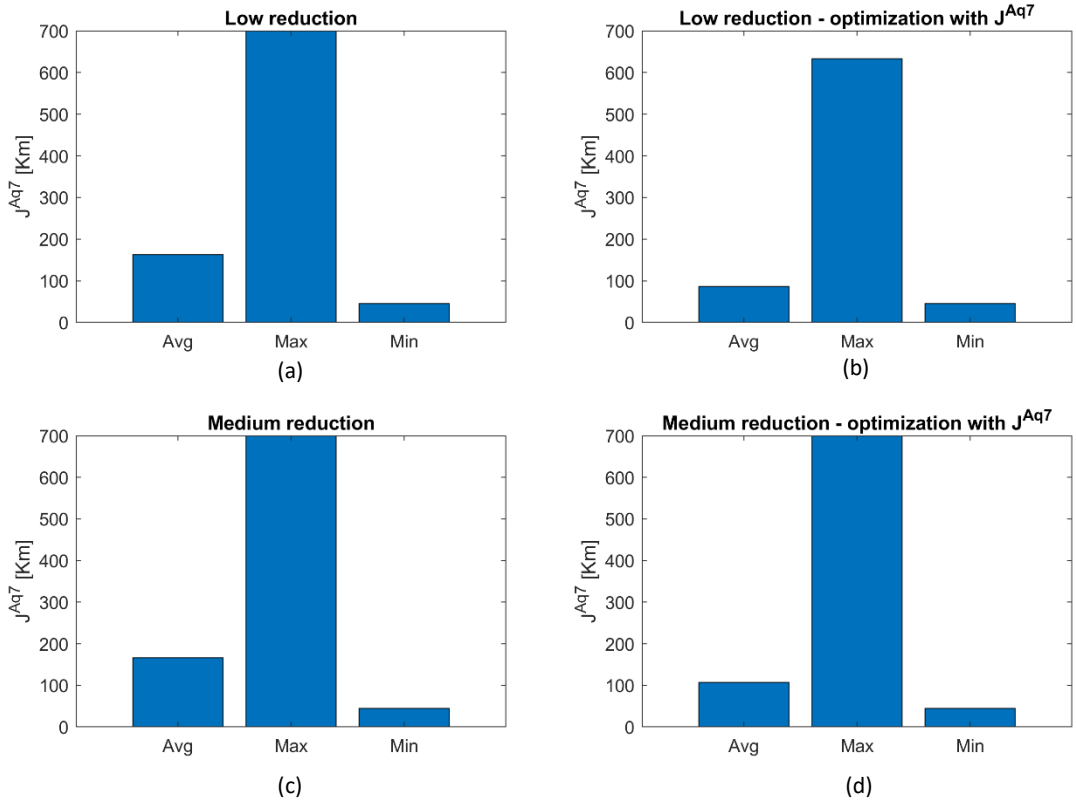

Figure 13 – Average, Maximum and minimum values of the J^{Aq7} indicator for the four water demand optimizations. (a) Low reduction optimization; (b) low reduction optimization with additional indicator; (c) medium reduction optimization and (d) medium reduction optimization with additional indicator.

Looking at the distribution of lettuce production in the four different optimisations (Figure 14), the two new optimizations show a higher production in and around district 8, where Cairo is located. Conversely, the old optimizations show a more evenly spatial distribution of lettuce production, generally higher in the Delta area. If the previous optimisation already showed good results by favouring the use of aquaponics in the Delta, where most of the Egyptian population is concentrated, the new optimisation with the additional objective shows even more robust results by concentrating most of the lettuce production in Cairo.

Finally, we compare the median values of the J^{Aq7} indicator for *traditional* solutions, i.e., those that do not employ aquaponics, and *innovative* solutions, i.e., those where aquaponics is used. From the comparison (Figure 15), we note that lower median values are obtained in the *innovative* solutions, the solutions in which aquaponics is used are more robust with respect to pandemic risk. Indeed, aquaponics makes it possible to grow lettuce and other vegetables within urban centres, so that in the case of events such as lockdowns, the food supply remains more accessible. By optimising the system with the additional J^{Aq7} indicator, we are able to achieve even more robust solutions (Figure 15b and d) where lettuce production is on average closer to the most densely populated areas.

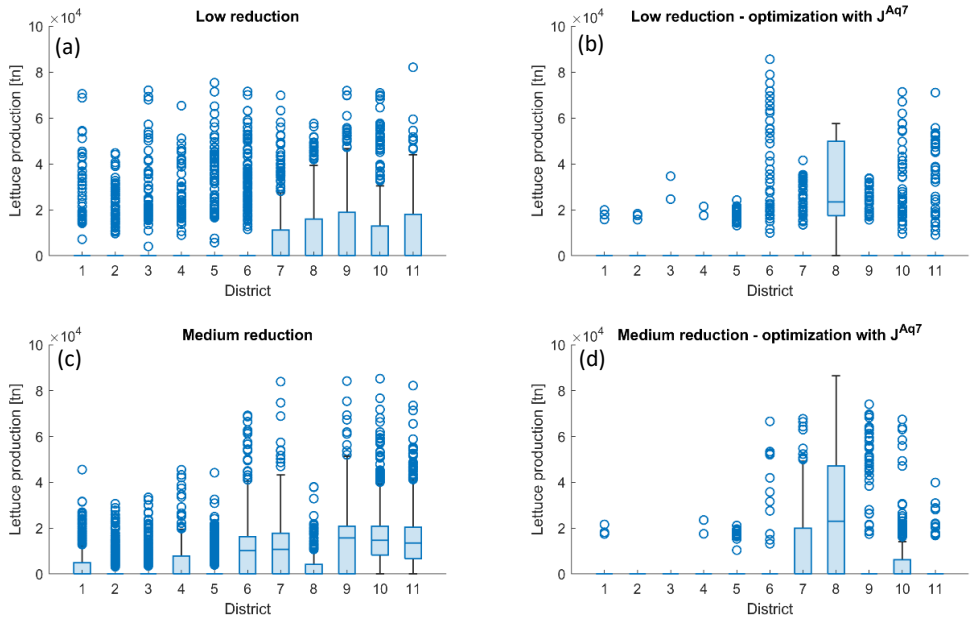

Figure 14 – Lettuce production in the eleven districts for the four water demand optimizations. (a) *Low reduction* optimization; (b) *low reduction* optimization with additional indicator; (c) *medium reduction* optimization and (d) *medium reduction* optimization with additional indicator.

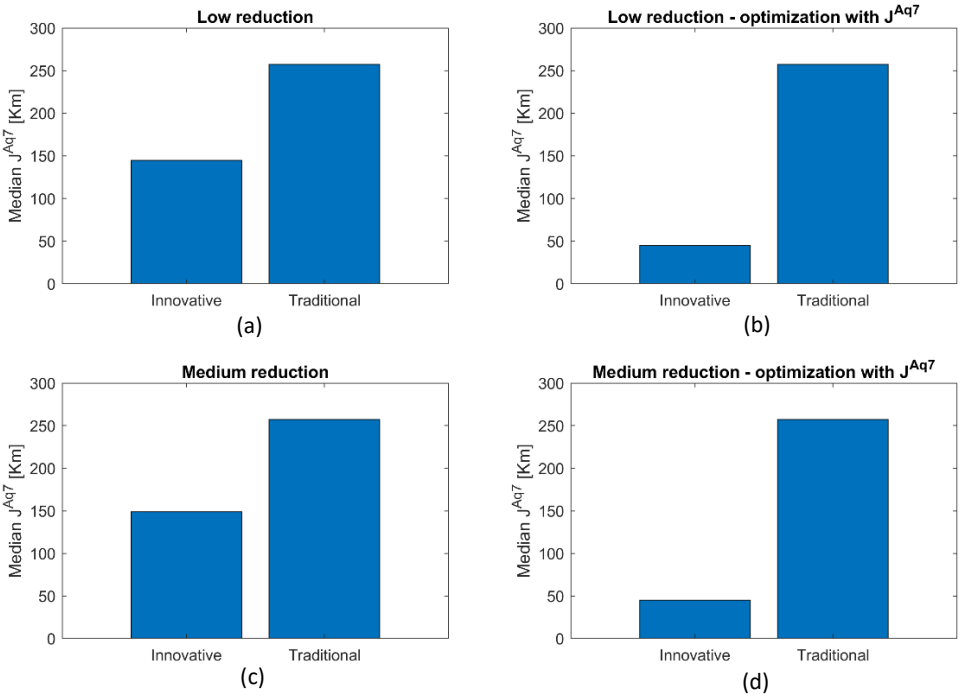

Figure 15 – Comparison of the median value of the indicator J^{Aq7} between the *innovative* and *traditional* solution for the four optimizations: low water reduction (a), low water reduction with the introduction of the additional indicator J^{Aq7} (b), for medium water reduction (c) and medium water reduction with the introduction of the additional indicator J^{Aq7} (d).

5. CONCLUDING REMARKS

In this deliverable we analysed the robustness to climate change and population growth of the optimal Water-Energy-Food-Ecosystem (WEFE) portfolios found through optimization of the strategic NRB model in D4.3. We also analysed the robustness of the planning portfolios for the introduction of measures such as reuse, groundwater, aquaponics and desalination to reduce Egypt's demand water. We used the framework introduced by[2] to stress test two efficient pathways found in D4.3 against a large ensemble of future scenarios of streamflows and water demand. The ensemble was generated from different SSPs and RCPs and consists of a very large set of future projections of population growth and climate change. The results obtained in the simulation of the NRB's operational system over the large ensemble show a large variation in indicators values compared to the original solutions. These results are justified by the wide variability of the input variables.

The hydroelectric production on a basin scale, as well as the individual productions of the three dams GERD, MER and HAD have a uniform distribution and increase linearly as inflows increase. As it is easy to see, hydroelectric production is closely linked to the inflow of the Nile, more water there is available, more energy can be produced. In contrast, the deficit values of Sudan and Egypt vary unequally, and are more concentrated on low deficit values. In particular, the deficit values in Sudan always remain at low values, showing a high level of robustness of the two solutions with respect to this indicator. In contrast, the deficit in Egypt tends to vary more widely, reaching high maximum values. This behaviour is justified by the high population growth in most future scenarios, which will directly affect the country's water demand. For the two irrigation deficits, a strong correlation with inflows can also be discerned, again, high inflows result in good indicator performance and vice versa. As for hydropower production, the relationship is linear, in this case we were also able to identify a minimum threshold of inflow below which the system will need to be reoperated as the two solutions become inefficient. In general, we found from this analysis that variation in inflows is the main driver influencing the performance of the indicators. Compared to the different scenarios considered, the RCP8.5-SSP5 scenario appears to be the most critical, resulting in the worst hydropower production performance and higher deficit in Egypt. This is easily explained by the fact that this scenario is the most affected by climate change, with higher temperature increases and higher reduction of precipitation. Exceptions are the results identified for the deficit in Sudan for which the most critical scenario is RCP4.5-SSP2. Regarding the downstream system, the identified solutions show robustness with most simulations requiring an increase in planning efforts of no more than 30% compared to the original solution.

Finally, we analysed the robustness of the identified solutions with respect to pandemic risk. To do this, we assessed the average distance of food production from the most densely populated areas. The results show that the use of aquaponics can increase the robustness of the system with respect to pandemic risk. In fact, this innovative form of agriculture makes it possible to cultivate crops in or near cities, as it does not require the use of large cultivated areas, unlike traditional agriculture. In this way, it is possible to bring food production and workplaces closer to urban centres, a great advantage in events such as lockdowns that restrict the possibility of movement.

6. REFERENCES

1. Maier, H. R. *et al.* Evolutionary algorithms and other metaheuristics in water resources: Current status, research challenges and future directions. *Environmental Modelling & Software* **62**, 271–299 (2014).
2. Hadka, D., Herman, J., Reed, P. & Keller, K. An open source framework for many-objective robust decision making. *Environmental Modelling & Software* **74**, 114–129 (2015).
3. Matalas, N. C. & M. B. Fiering. Climate, Climatic Change, and Water Supply. *Climate, Climatic Change, and Water Supply* (1977) doi:10.17226/185.
4. Difrancesco, K. N. & Tullos, D. D. Flexibility in Water Resources Management: Review of Concepts and Development of Assessment Measures for Flood Management Systems. *JAWRA Journal of the American Water Resources Association* **50**, 1527–1539 (2014).
5. Walker, W. E., Haasnoot, M. & Kwakkel, J. H. Adapt or Perish: A Review of Planning Approaches for Adaptation under Deep Uncertainty. *Sustainability 2013, Vol. 5, Pages 955-979* **5**, 955–979 (2013).
6. Lempert, R. J. & Beckman Center, M. A new decision sciences for complex systems. *Proceedings of the National Academy of Sciences* **99**, 7309–7313 (2002).
7. Brown, C., Ghile, Y., Laverty, M. & Li, K. Decision scaling: Linking bottom-up vulnerability analysis with climate projections in the water sector. *Water Resour Res* **48**, (2012).
8. Culley, S. *et al.* A bottom-up approach to identifying the maximum operational adaptive capacity of water resource systems to a changing climate. *Water Resour Res* **52**, 6751–6768 (2016).
9. Matrosov, E. S., Woods, A. M. & Harou, J. J. Robust Decision Making and Info-Gap Decision Theory for water resource system planning. *J Hydrol (Amst)* **494**, 43–58 (2013).
10. Reed, P. M., Hadka, D., Herman, J. D., Kasprzyk, J. R. & Kollat, J. B. Evolutionary multiobjective optimization in water resources: The past, present, and future. *Adv Water Resour* **51**, 438–456 (2013).
11. Mahmoud, M. *et al.* A formal framework for scenario development in support of environmental decision-making. *Environmental Modelling & Software* **24**, 798–808 (2009).
12. Groves, D. G. & Lempert, R. J. A new analytic method for finding policy-relevant scenarios. *Global Environmental Change* **17**, 73–85 (2007).
13. Giuliani, M. & Castelletti, A. Is robustness really robust? How different definitions of robustness impact decision-making under climate change. *Clim Change* **135**, 409–424 (2016).
14. Wald, A. Statistical Decision Functions. *London/New York: Chapman & Hall.* (1950).
15. Maier, H. R. *et al.* An uncertain future, deep uncertainty, scenarios, robustness and adaptation: How do they fit together? *Environmental Modelling & Software* **81**, 154–164 (2016).
16. Savage, L. J. The Theory of Statistical Decision. *J Am Stat Assoc* **46**, 55–67 (1951).
17. Simon, H. A. Dynamic Programming Under Uncertainty with a Quadratic Criterion Function. *Econometrica* **24**, 74 (1956).
18. Saltelli Andrea *et al.* Global Sensitivity Analysis: The Primer. in (2008).
19. Bergström, S. The HBV model. *Computer models of watershed hydrology.* 443–476 (1995).
20. Ševcíková, H. & Raftery, A. E. bayesPop: Probabilistic Population Projections. *J Stat Softw* **75**, (2016).

21. Raftery, A. E., Li, N., Ševčíková, H., Gerland, P. & Heilig, G. K. Bayesian probabilistic population projections for all countries. *Proceedings of the National Academy of Sciences* **109**, 13915–13921 (2012).
22. Chiarelli, D. D. *et al.* The green and blue crop water requirement WATNEEDS model and its global gridded outputs. *Scientific Data 2020 7:1* **7**, 1–9 (2020).
23. Quinn, J. D. *et al.* Exploring How Changing Monsoonal Dynamics and Human Pressures Challenge Multireservoir Management for Flood Protection, Hydropower Production, and Agricultural Water Supply. *Water Resour Res* **54**, 4638–4662 (2018).
24. Marani, M., Katul, G. G., Pan, W. K. & Parolari, A. J. Intensity and frequency of extreme novel epidemics. *Proc Natl Acad Sci U S A* **118**, e2105482118 (2021).